A&A 485, 787–795 (2008)
DOI: 10.1051/0004-6361:20079341

Astronomy & Astrophysics

The serendipituous discovery of a short-period eclipsing polar in 2XMMp⋆

J. Vogel[1], K. Byckling[2], A. Schwope[1], J. P. Osborne[2], R. Schwarz[1], and M. G. Watson[2]

[1] Astrophysikalisches Institut Potsdam, An der Sternwarte 16, 14482 Potsdam, Germany
e-mail: jvogel@aip.de
[2] Department of Physics and Astronomy, University of Leicester, Leicester LE1 7RH, UK

Received 29 December 2007 / Accepted 9 April 2008

ABSTRACT

We report the serendipituous discovery of the new eclipsing polar 2XMMp J131223.4+173659. Its striking X-ray light curve attracted immediate interest when we were visually inspecting the source products of the 2XMMp catalogue. This light curve revealed its likely nature as a magnetic cataclysmic variable of AM Herculis (or polar) type with an orbital period of ~92 min, which was confirmed by follow-up optical spectroscopy and photometry. 2XMMp J131223.4+173659 probably has a one-pole accretion geometry. It joins the group of now nine objects that show no evidence of a soft component in their X-ray spectra despite being in a high accretion state, thus escaping ROSAT/EUVE detection. We discuss the likely accretion scenario, the system parameters, and the spectral energy distribution.

Key words. X-rays: stars – stars: binaries: eclipsing – stars: novae, cataclysmic variables – X-rays: binaries

1. Introduction

Magnetic cataclysmic variables (mCVs) of the AM Herculis type are close binaries consisting of a magnetic white dwarf and a late-type main-sequence star in synchronous rotation (see Warner 1995, for a comprehensive overview). The late-type star loses matter via Roche-lobe overflow that initially follows a ballistic trajectory and eventually is guided by strong magnetic fields towards the polar regions of the white dwarf. The accretion plasma cools via X-ray bremsstrahlung and optical cyclotron radiation. A strong soft X-ray reprocessing component has been observed in many systems. This key feature, together with strong variability, gave the field a strong boost by the detection of about 45 new objects in EUVE/soft X-ray all-sky surveys (e.g. Beuermann & Burwitz 1995; Schwope et al. 2002a) compared to about 20 known before ROSAT/EUVE. With no wide-angle, soft X-ray survey telescope in space, new detections have become very infrequent since the 90's.

The public release of the Sloan Digital Sky Survey opened a new discovery channel. In a series of papers, Szkody et al. (2007, and references therein) presented the serendipituous CV content of the SDSS-sky. Among the several hundred CVs, approximately a dozen magnetic objects were found. This small fraction is probably more representative of the underlying population. All the new systems are faint at optical and X-ray wavelengths. A new class of low-accretion rate objects (formerly termed LARPs, Schwope et al. 2002b) in permanent low states was discovered by this route. The implied mass accretion rates revealed wind accretion instead of Roche-lobe overflow as the interaction channel, thus qualifying those 8 objects as magnetic pre-cataclysmic variables (Schmidt et al. 2005; Vogel et al. 2007).

Since the launch of Chandra and XMM-Newton, several large-scale optical identification programs have been started (e.g. Champ, Champlane, AXIS, XBS). Not surprisingly, due to their small survey area compared with ROSAT and EUVE, none of these led to the discovery of any new magnetic CVs. All the public XMM-Newton observations have been processed and surveyed by the XMM-Newton Survey Science Centre (SSC). The latest edition of the XMM catalogue, 2XMM, was made available in August 2007 (Watson et al. 2007, in preparation), its less elaborated predecessor, termed 2XMMp, was published in July 2006. The common feature of both catalogues is that the X-ray spectra and light curves were prepared and published as standard source products for objects with more than 500 source photons. Visual inspection of all the light curves led to the serendipituous discovery of 2XMMp J131223.4+173659 (for brevity 2XMM1312 in the following). The source stuck out as a bright and prominently variable object showing periodic modulations in its X-ray flux in the field of HD 114762, which is a high-proper motion star. Optical follow-up observations secured the tentative identification as an mCV. We present the analysis of the initial X-ray observations, and the spectroscopic and photometric follow-up.

2. Observations

2.1. XMM-Newton X-ray and UV observations

XMM-Newton observed the field of HD 114762 (OBSID 0200000101) for almost 32 ks on June 28, 2004. The observations were performed in full window imaging mode with all three cameras through the medium filter. All the X-ray and optical observations obtained are summarised in Table 1. Routine processing for the production of 2XMMp revealed the brightest X-ray source in the field at position RA, Dec (2000) = $13^h12^m23.46^s$, $+17^d36'59''.5$, with an error of 0.36 arcsec. The

⋆ Based on observations obtained with XMM-Newton, an ESA science mission with instruments and contributions directly funded by ESA Member States and NASA.

Table 1. Log of X-ray and optical observations.

Date (Y/M/D)	Instrument	Total duration [ks]	Sampl. time [s]
28/06/2004	XMM-PN	29.4	
	XMM-MOS1	31.6	
	XMM-MOS2	31.6	
	XMM OM-UVW1	0.8	
	XMM OM-UVM2	1.3	
	XMM OM-UVW2	1.4	
14/02/2007	CAHA 2.2 m CAFOS	8.7	440
19/03/2007	CAHA 2.2 m (R)	14	45

source was detected at an off-axis angle of ~6.3 arcmin. The three EPIC detectors detected more than 9500 photons from the source corresponding to a mean count rate of 0.304 ± 0.003. The standard products, i.e. the X-ray image, the DSS finding chart, the X-ray spectra, and the X-ray light curves, were automatically generated and visually inspected.

The PN X-ray light curve showed a striking behaviour with a periodic on/off pattern on a time-scale of ~90 min. The peak count rate reached 0.6 s^{-1} during the bright phase. Five bright phases were covered by the observations. They were each disrupted by a short (~300 s) eclipse-like feature. The shape of the light curve in general, its periodic behaviour, and the possible eclipse in the bright phase, were all reminiscent of a synchronously rotating magnetic CV (e.g. Schwope et al. 2001; Osborne et al. 1988), i.e., a so-called polar or *AM Herculis* star. In AM Her systems, there is an X-ray emitting accretion region near one or both of the magnetic poles of the white dwarf. The region may be eclipsed by the secondary and self-eclipsed by the white dwarf, and thus the variability seen in the light curves of AM Her systems can be due to the eclipsing of the emission area. Prior to the eclipse the light curve shows a dip, a feature also found in AM Her stars and caused by absorption of the softer X-rays when the emitting accretion region becomes eclipsed by the accretion stream. This striking light curve triggered a more detailed analysis of the X-ray data and optical follow-up to secure the tentative identification.

We reanalysed the X-ray data obtained with XMM-Newton using SAS version 7.0[1]. The usable energy range of the PN detector was extended down to 150 eV using *epreject*. Light curves and spectra were generated according to the SAS Manual. 2XMM1312 provided ~6200 photons in the EPIC PN detector, ~2000 photons in the EPIC MOS1 detector and ~1700 photons in the EPIC MOS2 detector. The MOS count rate reached ~0.25 s^{-1} during the bright phase. Nevertheless the MOS data were checked for pile-up using *epatplot* and were found to be not affected. The background-corrected, binned X-ray light curve of 2XMM1312, combining PN and MOS data, is reproduced in Fig. 1. The same data, folded and averaged over the orbital period of 91.85 min (see Sect. 3.1), are shown together with the optical light curve in Fig. 5. The mean X-ray spectrum is reproduced in Fig. 6 (we note that 2XMM1312 was not detected by ROSAT or by INTEGRAL). The XMM Optical Monitor (OM) was operated in default imaging mode with the *U*, *UVW1*, *UVM2* and *UVW2* filters. 2XMM1312 was detected in the *UVW1*, *UVM2* and *UVW2* filters, but not in *U*. Since the OM imaging mode does not allow for timing information, we get only an average flux for the corresponding phase interval. This information is summarised in Table 2.

[1] http://xmm.vilspa.esa.es/external/xmm_sw_cal/sas.shtml

Table 2. Count rates, fluxes and orbital phases of filter observations with the Optical Monitor (OM) onboard XMM-Newton.

Filter	λ_{eff} [Å]	Countrate	Flux (10^{-16}) [erg cm^{-2} s^{-1} $Å^{-1}$]	Orbital phase
UVW1	2910	0.264 ± 0.045	1.26 ± 0.21	0.25–0.40
UVM2	2310	0.099 ± 0.022	2.2 ± 0.5	0.97–0.21
UVW2	2120	0.039 ± 0.019	2.2 ± 1.0	0.52–0.77

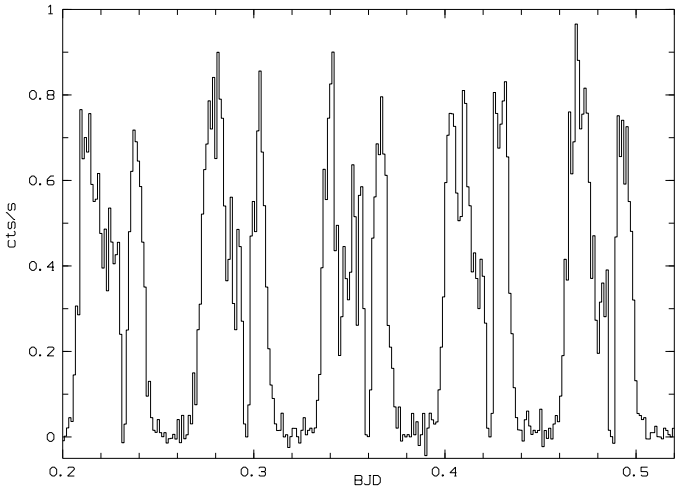

Fig. 1. Combined PN and MOS light curve with a binning of 110 s for the energy range 0.15−12.0 keV. Zeropoint is BJD = 2 453 185.0. For a phase folded light curve see Fig. 5.

2.2. Optical observations from Calar Alto

The X-ray position of 2XMM1312 was found to be coincident with the blue object SDSS J131223.48+173659.1 having *ugriz* magnitudes of 19.66, 19.69, 19.76, 19.81, 19.83, respectively. A finding chart of the field around the new CV is reproduced in Fig. 2.

2.2.1. Time-resolved low-resolution spectroscopy

Optical low-resolution spectroscopy was performed with the 2.2 m telescope at Calar Alto on February 16, 2007 between UT 03:05−05:30. The telescope was equipped with the low-resolution spectrograph and the CAFOS camera. The B-400 grism was used as disperser resulting in spectra with full coverage of the optical range from 3500−9500 Å with a resolution of ~28 Å (*FWHM*). A sequence of 20 spectra were taken with individual exposure times of 5 min each. Despite stable weather conditions, the object SDSS J131223.75+173701.2 located 4.4 arcsec NE to the candidate (*ugriz* = 20.72, 19.84, 19.67,19.59, 19.37) was put on the spectrograph's slit to correct for slit losses and variable seeing. The observations were accompanied by exposures of HgHeRb arc lamp spectra for wavelength calibration and of the standard star BD +75 325 for calibration of the instrumental response.

Data reduction was performed with ESO-MIDAS[2]. A two-step procedure was applied to achieve spectrophotometric results for the candidate CV. Firstly, a wavelength-independent correction factor was derived from the slightly varying signal of the second object on the slit and applied to the spectra of

[2] http://www.eso.org/sci/data-processing/software/esomidas/

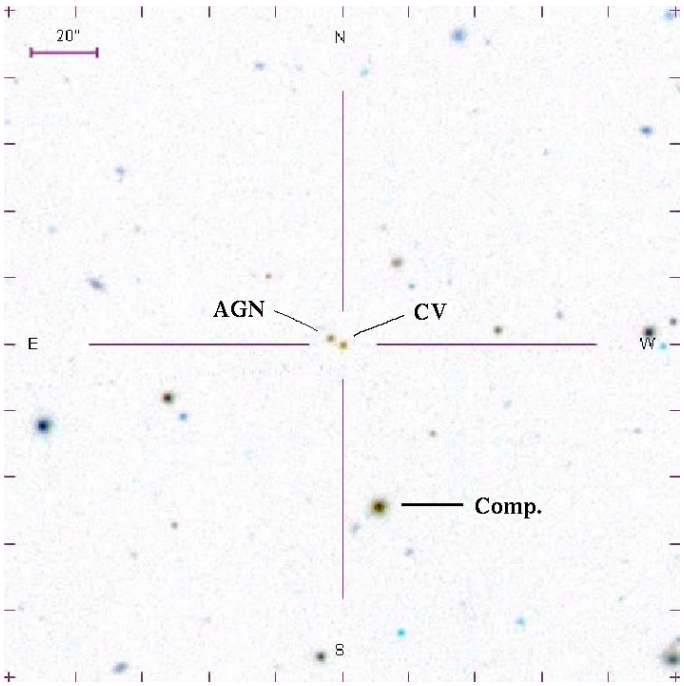

Fig. 2. Finding chart of 2XMM1312 created with the SDSS finding chart tool. The new CV, the nearby AGN and the comparison star used for differential photometry are marked.

the target. Secondly, the mean spectrum of the comparison object was folded through SDSS-filter curves and differential magnitudes with respect to the SDSS tabulated values computed. These were fitted with a second-order polynomial as a function of wavelength and the correction function applied to the spectra of the CV.

The mean spectrum of the CV candidate is reproduced in Fig. 3 and – together with the X-ray light curve – identifies 2XMM1312 as a magnetic CV of AM Herculis type. Approximate *BVR*-band light curves of the CV were constructed by folding the final spectra through the response curves of Bessel filters and are reproduced in Fig. 8. Those light curves also show an eclipse, there is one spectrum with a non-detection of the target resulting in an upper limit to the brightness of the object of $V \sim 21\overset{m}{.}5$.

The second object on the slit, which was used as a photometric calibration source, turned out to be a quasar at redshift $z = 2.43$ with strong and broad emission lines of Lyα, SiIV, CIV 1550, and CIII 1900. The mean spectrum of the QSO is reproduced in Fig. 4.

2.2.2. Time-resolved differential *R*-band photometry

Optical *R* band photometry was performed one month after the spectroscopy on March 19 between UT 00:32–04:25 with an exposure time of 30 s at the Calar Alto 2.2 m telescope. A total of 305 exposures were taken covering two and a half cycles of the binary and three eclipses. The comparison used for photometric calibration is marked in Fig. 2.

The phase-folded optical light curve of the CV is shown in Fig. 5 together with the X-ray light curve (see Sect. 3.1 for the ephemeris). A zoomed-in version of the same data centred on the optical eclipse is shown in Fig. 12. Similar to the X-ray light curve, the overall light curve shows a bright hump followed by a dip prior to the eclipse.

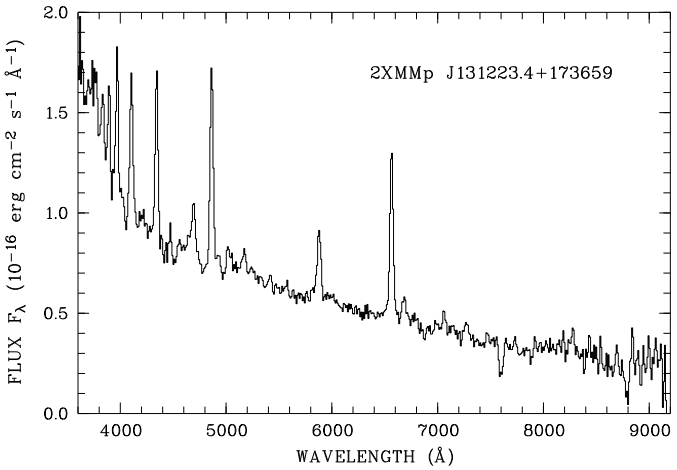

Fig. 3. Average spectrum of 2XMM1312 (=SDSS J131223.48+173659.1) obtained on February 16, 2007, with the CA 2.2 m telescope and CAFOS (total exposure 100 min).

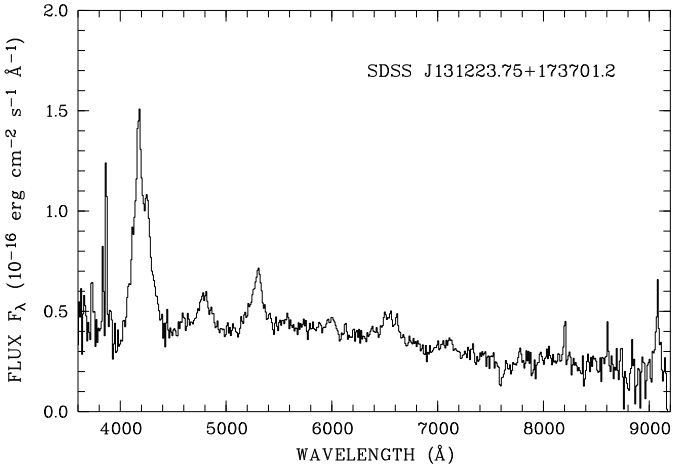

Fig. 4. Average spectrum of the quasar SDSS J131223.75+173701.2 obtained on February 16, 2007.

Out of the eclipse, the *R*-band brightness varied between $\sim 19\overset{m}{.}1$ and $\sim 19\overset{m}{.}4$. The CV was not detected in the individual exposures at the bottom of the eclipse. A stacked image using those 11 images was created. From the statistical analysis of that image we derived an upper limit of $22\overset{m}{.}3$ for the brightness of the secondary. The orbital period of ~92 min (see next section) implies a spectral type of M5.5 ± 0.5 (Beuermann et al. 1998). Using the absolute magnitudes from Kirkpatrick & McCarthy (1994) this results in a minimum distance of ~900 pc for a M5 and ~350 pc for a M6 spectral type.

3. Analysis and discussion

3.1. A combined X-ray/optical ephemeris

We found an eclipse in all three datasets obtained so far. This excludes anything else than an eclipse proper by the mass-donating secondary star. Here we make an attempt to combine the eclipse epochs from the three sets into one binary ephemeris. For the analysis of the X-ray data a combined light curve of all the three EPIC cameras with a binning of 5 s was used. The X-ray eclipse shows just the ingress and egress of the accretion spot and does not resolve any detail. The individual X-ray eclipse timings with an uncertainty equal to the bin size were used to determine the

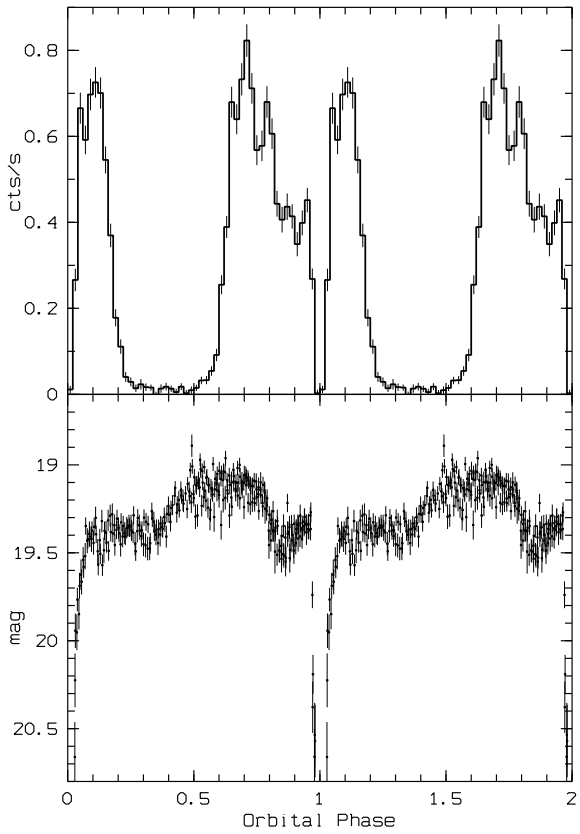

Fig. 5. *The upper panel* shows the phase folded X-ray light curve from 2004 composed of EPIC PN and MOS counts with a binning of 0.02 phase units. *The lower panel* shows the phase folded *R* band light curve from March 2007.

times of the mid-eclipses. The mean X-ray eclipse length resulting from the five individual eclipses is 329 ± 3 s.

The exposure time of the optical spectra was 300 s, but the last spectrum in our sequence of 20 did not yield a significant detection. Since the length of the X-ray eclipse is slightly longer than this exposure time, we assume that this spectrum is centred on the X-ray eclipse with the rather small uncertainty (compared to the exposure time) of 60 s only.

The mean eclipse light curve from the *R* band photometry (see Fig. 12) clearly shows the ingress and the egress of the white dwarf and/or the spot and the accretion stream. Since the individual eclipses do not resolve these details, we used the mean eclipse light curve – phase folded with the period derived from the X-ray data (see below) – to determine the flux level for mid-ingress and mid-egress of the white dwarf/spot. For the individual eclipses we interpolated between single exposures to get the timings for the chosen flux level, and thus the times of the ingress and egress of the spot.

The five consecutive X-ray eclipses were used to derive a preliminary period of 0.06378(3) d that could be used to connect the eclipse times obtained from spectroscopy and photometry at Calar Alto without cycle count alias. A linear regression to the four optical eclipse times yielded a period of 0.063785(1) d. This turned out to be sufficiently accurate to connect the 2004 XMM-Newton X-ray data with the optical data from 2007, again without cycle count alias. A linear regression using all nine eclipse epochs revealed the finally accepted eclipse ephemeris of:

$$\mathrm{BJD(UT)} = 2\,453\,185.23204(4) + E \times 0.06378527(1) \qquad (1)$$

Table 3. Mid-eclipse timings.

Observation	Time [BJD]	Cycle	O–C [s]
XMM EPIC 2004	2 453 185.23203(8)	0	–0.6
XMM EPIC 2004	2 453 185.29585(8)	1	2.5
XMM EPIC 2004	2 453 185.35959(8)	2	–1.7
XMM EPIC 2004	2 453 185.42345(8)	3	4.3
XMM EPIC 2004	2 453 185.48715(8)	4	–2.3
CAHA Spec 2007	2 454 146.7313(7)	15074	8.6
CAHA Phot 2007	2 454 178.5600(4)	15573	–4.3
CAHA Phot 2007	2 454 178.6240(4)	15574	14.3
CAHA Phot 2007	2 454 178.6875(4)	15575	–10.4

which corresponds to an orbital period of $P_{\rm orb}$ = 91.85079(1) min. Numbers in parentheses indicate the uncertainties in the last digits. All phases in this paper refer to the linear ephemeris of Eq. (1). The mid-eclipse times for all the eclipses are given in Table 3.

3.2. The X-ray spectrum

The PN and MOS X-ray spectra were extracted according to the SAS manual. The data were binned to at least 20 cts/bin. The spectral fits were generated using Xspec[3]. A good fit to the PN and MOS mean spectra (see Fig. 6) was obtained with an absorbed MEKAL model with $\chi^2_\nu = 1.01$, and resulted as a plasma temperature of $kT = 29(8)$ keV and a column density of $N_{\rm H} = 2.0(6) \times 10^{20}$ cm^{-2}. As a comparison, a Galactic column density of $N_{\rm H} = 1.87 \times 10^{20}$ cm^{-2} was obtained with the *nh* program, which is provided by the FTOOLS package[4]. The target coordinates correspond to a galactic latitude of 79°, so this value seems still reasonable with respect to the estimated distance. The unabsorbed flux is 1.4×10^{-12} erg s^{-1} cm^{-2} in the energy range 0.15–12.0 keV. We also experimented with a more complex absorption component using the *pcfabs* model in Xspec, but in this model the parameters of the absorber were not constrained by the data. The above model parameters results in a predicted ROSAT count rate of 0.03 ct/s, slightly below the RASS detection limit of 0.05 ct/s, which explains the non-detection during the RASS if we assume a comparable accretion state for the XMM and the ROSAT observation and even if we assume that the RASS scans covered the bright phase.

We also created a combined spectrum for the bright phase intervals before the absorption dip occurs. This corresponds to the orbital phase interval of ~0.6–0.8. The phase intervals were visually selected for each individual orbit. A fit with an absorbed MEKAL model resulted in a plasma temperature of $kT = 14(4)$ keV and a column density of $N_{\rm H} = 2.1(7) \times 10^{20}$ cm^{-2} ($\chi^2_\nu = 1.01$). The spectral fit together with the confidence range is shown in Fig. 7. Since at the given phase interval the accretion region is directly exposed towards the observer, a fit to this spectrum reveals the most likely plasma temperature. The unabsorbed flux is 2.8×10^{-12} erg s^{-1} cm^{-2} in the energy range 0.15–12.0 keV, the bolometric flux 3.8×10^{-12} erg s^{-1} cm^{-2} that results in an accretion luminosity of $L_{\rm accr} \geq 0.55 \times 10^{32}\ d^2_{350}$ erg s^{-1}, where d_{350} is the distance in units of 350 pc. The luminosity can be compared to the expected accretion luminosity. According to the standard theory, the mass transfer below the period gap is driven solely by the angular momentum loss due to gravitational radiation. The resulting mass transfer rate for the derived orbital period would be

[3] http://heasarc.gsfc.nasa.gov/docs/xanadu/xspec/
[4] http://heasarc.gsfc.nasa.gov/docs/software/ftools

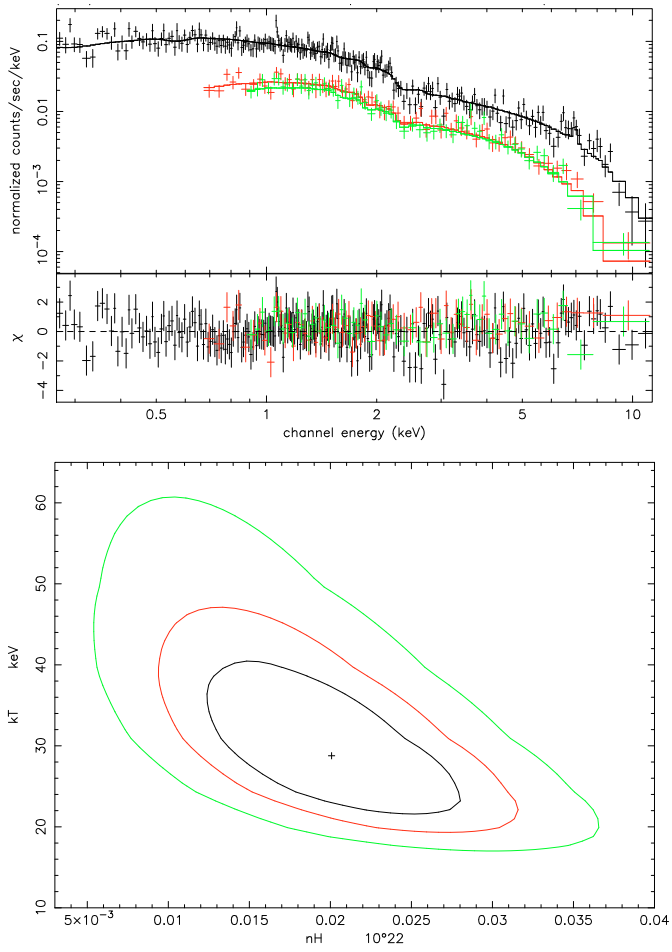

Fig. 6. Spectral fit of the combined PN and MOS mean spectra with an absorbed MEKAL model, together with the confidence range (0.68, 0.90 and 0.99) as a function of the MEKAL temperature and the column density of the interstellar absorption.

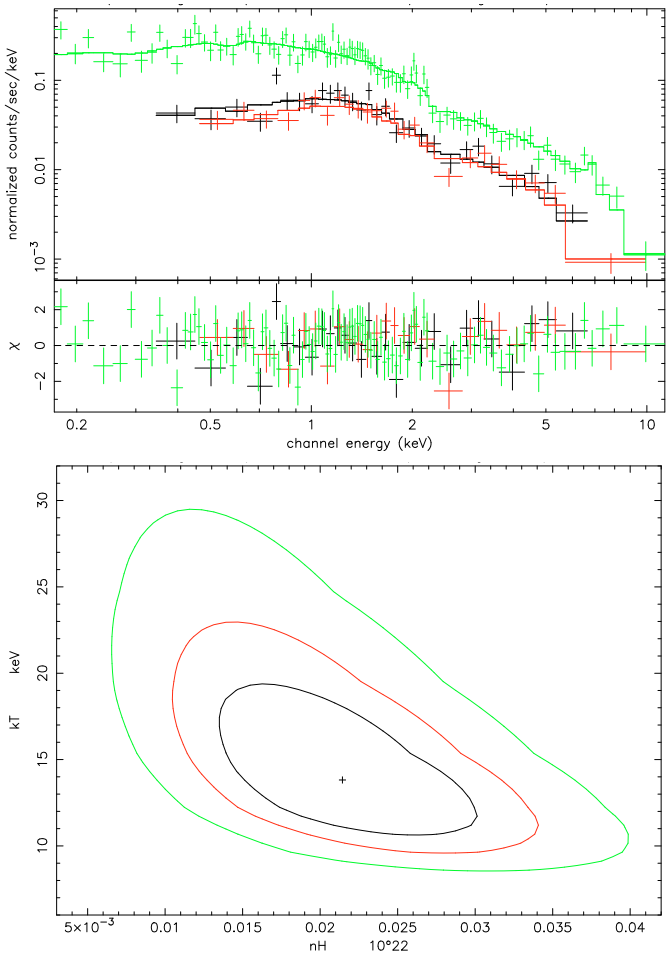

Fig. 7. Spectral fit of the combined PN and MOS spectra of the X-ray bright phase before the absorption dip with an absorbed MEKAL model, together with the confidence range (0.68, 0.90 and 0.99) as a function of the MEKAL temperature and the column density of the interstellar absorption. The bright phase interval was selected individually for each of the five orbits. Note the different scaling of the y axis compared to Fig. 6.

$\dot{M} = 2.8 \times 10^{-11}\ M_\odot\ \mathrm{yr}^{-1}$ (Warner 1995) and lead to an accretion luminosity of $L_{\mathrm{acc}} = 1.6 \times 10^{32}$ erg s^{-1} (for the used masses of white dwarf and secondary see Sect. 3.6). This is in good agreement with the actually measured luminosity.

Contrary to the general assumption of accretion in AM Her stars, which emerged from the analysis of the large body of e.g. ROSAT data, the X-ray spectrum of this object shows no evidence for the presence of a distinct soft component. In most AM Her stars, the soft component originates from the heated atmosphere of the white dwarf around the accretion spot. Thus, 2XMM1312 joins the group of now 9 out of ~80 polars without a soft component (Ramsay & Cropper 2007). A likely explanation for the non-detection of the soft component is its low temperature which shifts the emission towards lower energies not covered by the X-ray cameras of the XMM-Newton. To derive upper limits for the soft component, we model this component with a black body spectrum based on the constraints that the Rayleigh-Jeans tail of the assumed black body must not exceed the observed spectral flux in the ultraviolet, and that the contribution of the soft component to the 0.15–0.30 keV band is less than 10%. With a 0.6 $M_\odot$ white dwarf and a distance of 900 pc, the fraction of the white dwarf surface that is covered by the pole cap falls below 10^{-3} for a temperature above 15 eV that is considered as the upper temperature limit.

This temperature is at the lower end of the otherwise observed temperatures for the soft component, but is still too high to contribute in the UV. To test the energy balance of the reprocessed component we assumed a black body with a temperature of 10 eV, providing 10% of the flux in the 0.15–0.30 keV band (see Fig. 9). The resulting contribution in the *UVW2* filter is still less than one fourth, but the integrated flux exceeds the flux of the bremsstrahlung component by a factor of hundred. Thus, the UV and X-ray observations give no constraints for the maximum flux contribution of the soft component that could lead to a conflict with the standard model. In summary, the missing soft component is not really puzzling. If the accretion occurs over a large fraction of the white dwarf surface, the temperature of the pole cap would be lower than observed in polars with soft component. The lower temperature simply shifts the observable soft component towards the EUV, out of the XMM band pass.

3.3. The X-ray eclipse emission

The EPIC light curve shows a residual X-ray flux of $F_{\mathrm{X}} = 1.2 \times 10^{-14}$ erg cm^{-2} s^{-1} when the white dwarf and the accretion region are eclipsed by the secondary. The origin of this emission is not obvious at first glance. 2XMM1312 is accompanied by SDSS J131223.75+173701.2 at a distance of 4.4 arcsec. The

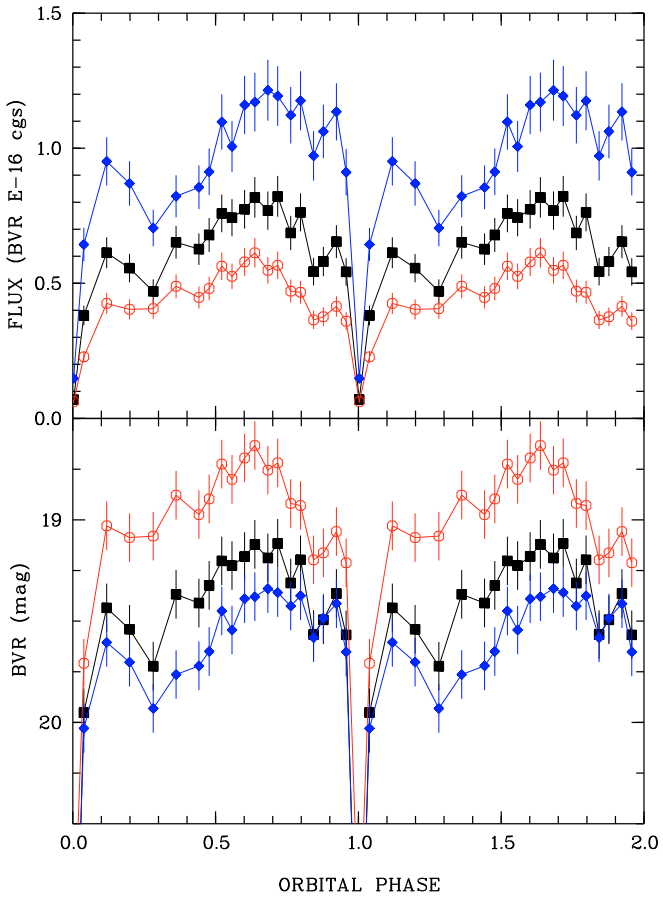

Fig. 8. Optical light curves in *BVR* (in descending order for *the upper plot* and ascending order for *the lower plot*) bandpasses determined from flux-calibrated phase-resolved spectra of February 16, 2007. We estimated the errors from our reduction procedure to ~0.12^{m}.

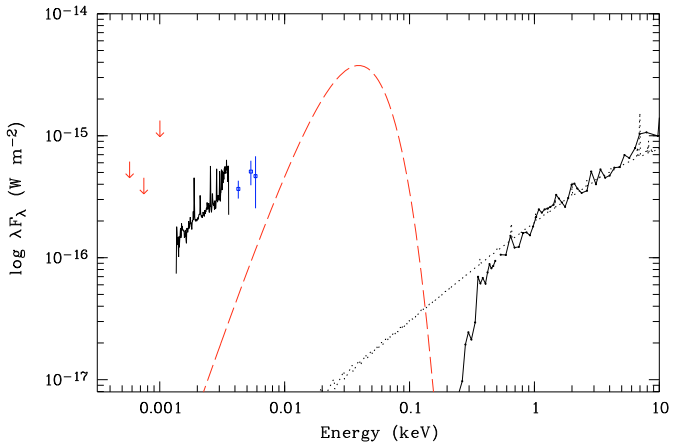

Fig. 9. Spectral energy distribution with all available data: 2MASS upper limits (arrows on the left), CAHA mean spectrum (next to the arrows), XMM OM (next to the long dashed line) and XMM EPIC spectrum (on the right). Overplotted (long dash) is a 10 eV black body providing a negligible fraction of 10% of the observed soft X-ray flux (see Sect. 3.2 for a discussion of this component) and the MEKAL model spectrum (dotted line).

spectroscopic observations show that this object is a quasar at redshift $z = 2.43$. The quasar is not resolved in our XMM EPIC data, although quasars are known to be X-ray emitters. We tried two methods to distinguish between the two sources to clarify if the residual X-ray emission emerges from the AGN or from the corona of the secondary star (if the secondary is X-ray active at all).

Our first attempt was to spatially resolve the polar and AGN by using phase selected event lists for bright, faint and eclipse phase on which the SAS source detection was run. All three source positions found were the same within the error circles, which is not surprising since the distance between both sources is at the limit of the spatial resolution.

The next attempt was to use the properties of the spectral energy distribution. We computed the flux from the dozen photons during the eclipse, taking the interstellar absorption from the spectral fit above into account. The X-ray flux of $F_X = 1.2 \times 10^{-14}$ erg cm^{-2} s^{-1} was then compared with the optical flux. From the SDSS magnitudes of the AGN we computed a optical flux of $F_{opt} = 2.76 \times 10^{-14}$ erg cm^{-2} s^{-1} (Zombeck 1990). The ratio $F_X/F_{opt} = 0.4$ can be compared with the properties of other AGNs. For most AGNs F_X/F_{opt} is found to be between 1 and 10, but can also be one order of magnitude less, while for stars this ratio is mostly below 0.05 (Schwope et al. 2000). Ascribing the complete flux to the secondary, the X-ray flux transforms into a luminosity of $L_X = (1.8–11.6) \times 10^{29}$ erg s^{-1}. The assumed spectral type and the distances (see Sect. 2.2.2) lead to a bolometric luminosity of $L_{bol} = (3.18–3.43) \times 10^{30}$ erg s^{-1} (Leggett et al. 1996), and thus $L_X/L_{bol} \sim 0.3$ for an M5 and ~0.06 for an M6. This is orders of magnitudes above the value which could be expected for an active M dwarf (Pizzolato et al. 2003). As the assumed distance increases L_X and thus L_X/L_{bol} also increases, making the ratio even larger.

Therefore, we suggest to ascribe the residual X-ray emission during the eclipse to the AGN. Since the contribution from the AGN is rather small and the real flux contribution is uncertain, we neglect the contribution by the AGN for any further analysis of the X-ray data. Since we have more flux during the faint phase than during the time of the eclipse, there must be an additional contribution at this time. Either the self-eclipse is not complete or we see bremsstrahlung reflected from the accretion stream. Due to the low number of photons and the merged contribution from the quasar and the polar we could not make any viable conclusion from the hardness ratio.

3.4. The optical spectrum

The optical spectrum of 2XMM1312 clearly reveals its nature as a CV through the presence of a blue continuum with strong, superposed emission lines of H, HeI and HeII. In general, the optical spectra of CVs are a mixture of contributions by the photosphere of the white dwarf; the heated pole cap and the accretion spot on the white dwarf; cyclotron radiation from the cooling plasma and recombination radiation from the accretion stream; and the illuminated secondary. Some attempts to disentagle those components can be made by utilising the shape of the eclipse, extracting and comparing different bands, and by subtracting bright- and faint-phase spectra with the aim to single out one of those components. Apart from the eclipse proper the light curves in *BVR* bands are modulated by ~50% and show one bright hump with a colour-dependent phase of maximum emission. The shift between the *B* and *R* band humps could be caused by beaming properties of the cyclotron radiation that is more beamed at higher harmonics (shorter wavelengths). The difference between the average spectra in phase intervals 0.5–0.8 (brightest phase interval) and 0.2–0.4 (faint phase), however, displays just a smoothly varying blue continuum and does not

show any feature which could be associated with a cyclotron harmonic hump. The more likely explanation is to assume a different approach to explain the existence of the humps. The centre of the *B* band bright phase corresponds to the centre of the X-ray bright phase at phase ~0.9. Thus, the *B* band hump is likely to originate from the heated pole cap, while the *R* band hump can be explained by cyclotron origin (see Sect. 3.6). This implies a cyclotron component which contributes in the red and infrared, indicative of a rather low field strength of ~10–20 MG. Unfortunately, there was no indication of Zeeman split lines in the spectra that could be used to determine the magnetic field strength directly.

As a rough guess for the contribution of the cyclotron component, we computed the flux difference between the faint phase and the bright phase. This clearly is an upper limit for the cyclotron flux since it contains an undetermined fraction of atmospheric emission from the accretion-heated spot. Nevertheless, if we regard the contribution of 1.1×10^{-13} erg cm^{-2} s^{-1} during the bright phase as of pure cyclotron origin and apply a factor of 2 for correction of beaming properties and unobserved cyclotron features, one gets $F_{\rm cyc}/F_{\rm X} \leq 0.1$ that demonstrates the prevalence of plasma cooling via bremsstrahlung over cyclotron cooling and also indicates low field strength (Beuermann 2004).

3.5. Overall flux distribution

The spectral energy distribution with all available data is shown in Fig. 9. 2XMM1312 is not detected in 2MASS, thus an upper flux limit could be derived for the *JHK* bands. While the optical and the X-ray spectra represent the mean over the orbital cycle, the UV data points belong to specific orbital phases (see Table 2). According to the spectral energy distribution, it is clear that there is a strong flux contribution from the accretion stream in the UV. The *UVW1* filter covers just the faint phase, where the accretion spot is self-eclipsed and does not contribute. Assuming a low temperature white dwarf, the upper limit to the contribution of the white dwarf is given by the optical flux, whereas assuming a high temperature white dwarf, the upper limit is given by the flux in the *UVW2* band. A white dwarf model spectrum of $T = 20\,000$ K could provide ~70% of the flux in the *UVW1* band, and a $T = 11\,000$ K white dwarf ~60%. The remaining flux has to be provided by the accretion stream. To visualise the possible contribution of the soft component, a black body spectrum of $T = 10$ eV is also included in Fig. 9. The black body provides 10% of the X-ray flux in the energy band 0.15–0.3 keV.

3.6. Binary parameters and system geometry

The optical mean eclipse light curve in Fig. 12 indicates the ingress and egress of the white dwarf/accretion spot and the stream. The width of the optical eclipse is 320 ± 3 s compared to the X-ray eclipse length of 329 ± 3 s. The stream ingress lasts until phase 0.995 and the stream egress until phase ~1.08. We used the steep decline during the eclipse ingress as a consistency check for the binary distance as derived from the spectral type of the secondary. While the gradual decline is caused by the accretion stream, the steep decline represents the eclipse of the white dwarf and/or spot. Thus, the flux provided by the white dwarf alone must not exceed the step height of ~1.7×10^{-17} erg s^{-1} cm^{-2} Å^{-1}. With a mean white dwarf mass of $M_1 \sim 0.6\ M_\odot$ and a mean temperature of 16 000 K (Sion 1999), the implied distance is $d \geq 550$ pc, which is consistent with the distances derived in Sect. 2.2.2.

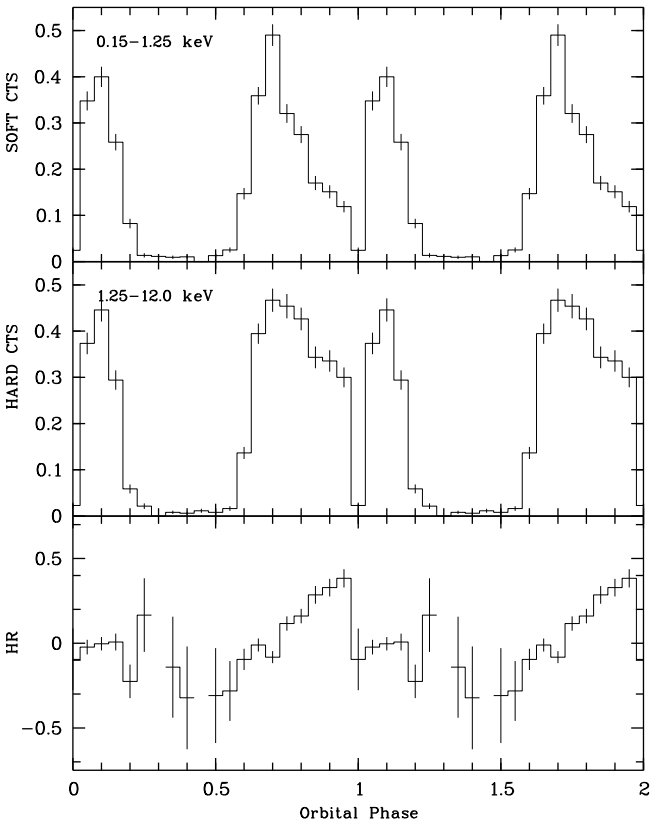

Fig. 10. PN light curve for soft (0.15–1.25 keV) and hard (1.25–12.0 keV) energy ranges together with the resulting hardness ratio. Soft and hard band contain approximately an equal number of photons (~3100).

Assuming the secondary fills its Roche-lobe and by using the $M - R$ relation from Knigge (2006) together with the period, we get a secondary mass of $M_2 \sim 0.09$, which is only weakly dependent on the mass ratio q. The mass of the secondary and the assumed white dwarf mass of $M_1 \sim 0.6$ yields a mass ratio of $q \sim 0.15$. The mass ratio, the orbital period, and the eclipse width determine the orbital inlination. Since the white dwarf is not resolved in our data, we used the mean spot eclipse width of 325 s to compute a $q - i$ relation that results at the inclination of $i \sim 83°$. Since the real white dwarf mass remains unknown, the derived inclination is just the approach of least prejudice, but hardly constrains the system geometry.

The X-ray bright phase is centred at phase 0.9 that gives the azimuth of approximately 36°. The length of the X-ray bright phase is about 0.62 phase units locating the accretion spot on the hemisphere most oriented towards earth. Since the length of bright phase depends on the inclination i and colatitude β of the accretion region, we get a constraint for the colatitude. Neglecting any height of the accretion column, the colatitude is $\beta \sim 20°$ for $i \sim 83°$, but correspondingly larger for a possible vertical or horizontal extent of the emission region.

Both the optical and X-ray eclipses are preceded by a dip. This is also found in other polars and is caused by absorption of X-rays when the accretion stream passes the line of sight to the emitting accretion region (Watson et al. 1987; Schwope et al. 2001) as is required if $i > \beta$. In this case, we expect to see a change in the hardness ratio since the photoelectric absorption cross-section is greater at lower energies. The hardness ratio together with the soft and hard X-ray light curve can be seen in Fig. 10. Interestingly, the hardness ratio shows a monotonic

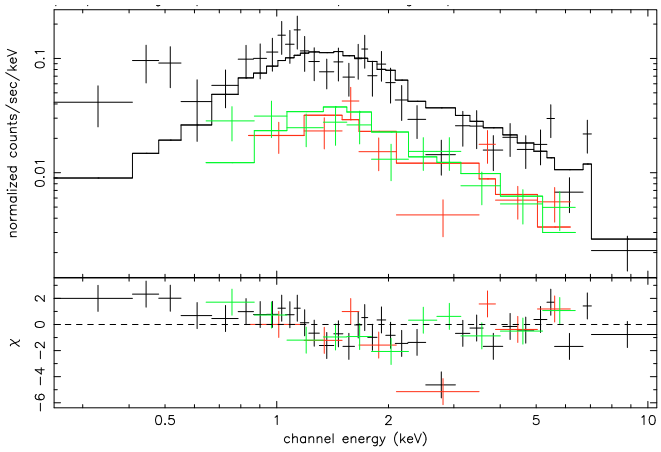

Fig. 11. Spectral fit of the combined PN and MOS spectra for the phase intervals of the absorption dip (visually selected for each orbit) with an absorbed MEKAL model. Plasma temperature and normalisation were fixed to the fitting values of the bright phase spectrum before the absorption dip.

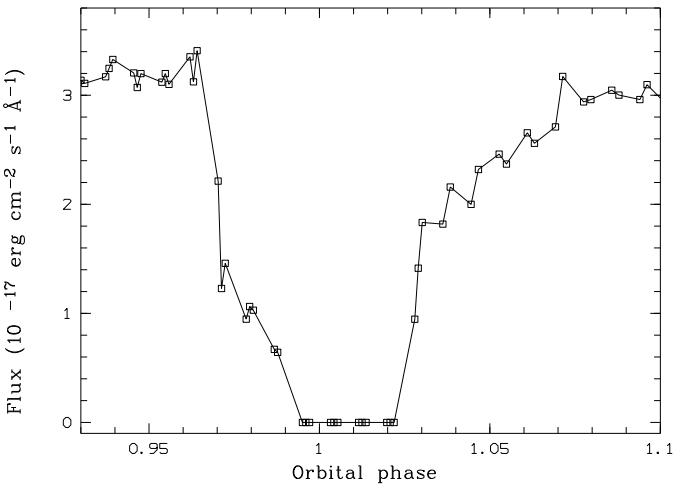

Fig. 12. Mean eclipse light curve from the optical *R* band observations on March 19 (errors are smaller than symbol size). Ingress and egress of accretion spot and accretion stream are clearly identifiable. Non-detections are set to zero.

increase from phase 0.75 until the beginning of the eclipse. If this is just due to the photoelectric absorption, the corresponding accretion stream has to be extended over a large range in azimuth and is more properly an accretion curtain than a well-defined stream. This could also be an explanation for the non-detection of the soft component of reprocessed origin. An extended accretion curtain leads to a bigger and thus lower temperature accretion region on account of the lower specific accretion rate. We searched for evidence of an extended accretion arc from the X-ray light curve at eclipse ingress and egress. Ingress and egress are safely shorter than 5 s and likely shorter than 3 s but the low number of counts does not allow to derive stringent limits. For comparison, in the similar system HU Aqr, ROSAT-observed eclipse egress lasts 1.3 s (Schwope et al. 2001).

To test whether the dip is caused by absorption of cold material, we tried to fit the X-ray spectrum of the phase intervals where the dip occurs. The plasma temperature and normalisation were fixed to the fitting values of the bright phase spectrum before the absorption dip (see Sect. 3.2). To ascertain whether the spectral change between the bright phase and the dip can be explained with additional absorption, the hydrogen column was left as a free parameter. With these constraints, a reasonable fit with a total $N_{\rm H} = 0.41(4) \times 10^{22}$ cm^{-2} and $\chi^2_\nu = 2.2$ was obtained.

Assuming a high inclination as derived above, the centre of the stream dip gives the azimuth of the threading region in the orbital plane. The X-ray dip is centred at phase ~0.9. This corresponds to an azimuth of ~54° of the threading region. The optical stream dip is centred at phase ~0.85, somewhat before the X-ray dip. The phase difference could either be due to a shifted spot location or a higher accretion rate compared to the X-ray observation, and thus an accretion stream coupling later in the orbital plane to the magnetic field.

The centre of the *R* band hump occurs at phase ~0.62, which is 0.3 phase units before the centre of X-ray bright phase. If we exclude a radical change in accretion geometry between the X-ray observation in 2004 and the optical observation in 2007, this can be explained by cyclotron beaming, meaning a cyclotron origin of the *R* band hump. With the spot location as derived above, the centre of the *R* band hump corresponds to the orbital phase where the spot just appears from the limb of the white dwarf. The optical hump starts at phase ~0.35, which is during the X-ray faint phase, and lasts until phase ~0.55. This suggests that the eclipse of the accretion column by the white dwarf is complete only in X-rays and partial at optical wavelength due to a high shock, so beamed cyclotron radiation is still seen, while the X-ray emitting region is hidden behind the white dwarf. The remaining puzzle is the missing second optical hump. With this explanation a second hump would be expected, when the spot disappears behind the limb of the white dwarf. The missing second hump implies a rather large angle between magnetic field vector and surface normal, which is hard to explain with a simple dipole geometry.

With the system parameters derived above, we modelled the extent of the accretion curtain for the given system and binary parameters and were able to reproduce the observed timings of the *R* band eclipse light curve. The long ingress phase of the curtain is due to the extended ballistic accretion stream which has its largest extent at an azimuth of ~60°.

4. Summary

We have presented the analysis of the newly discovered eclipsing polar 2XMM1312. The polar shows a hard X-ray spectrum with a plasma temperature of ~14 keV, but no sign of a soft component. The soft component is probably shifted to the EUV due to an extended accretion region and thus a cooler accretion region. The system has one active accretion spot on the hemisphere most oriented towards earth with an azimuth of ~36° and a low colatitude. The orbital period, 92 min, could be determined with a fairly high accuracy. The distance is likely to be ≥500 pc.

We could not directly determine the strength of the magnetic field, but the large extent of the ballistic stream and the properties of the cyclotron radiation suggest a rather low field strength of $B \leq 10$ MG. We suggest high-speed optical photometry observations with a large telescope to test our prediction of a large extended accretion arc and to determine the brightness and colour of the secondary in eclipse. We further suggest IR spectroscopy and polarimetry to directly determine the magnetic field strength. Finally, phase-resolved UV photometry would help to determine the temperature of the white dwarf and the size of the accretion spot, allow to further disentangle radiation components, and settle the question of the undetected soft component.

Acknowledgements. J.V. and R.S.C. are supported by the Deutsches Zentrum für Luft- und Raumfahrt (DLR) GmbH under contract No. FKZ 50 OR 0404. K.B. acknowledges funding from the European Commission under the Marie Curie Host Fellowship for Early Stage Research Training SPARTAN, Contract No. MEST-CT-2004-007512, University of Leicester, UK. J.O. acknowledges the support of PPARC. We thank the German-Spanish Astronomical Center at Calar Alto for allocating directors discretionary observing time and the Calar Alto staff for competent execution of the service mode observations.

References

Beuermann, K. 2004, in Magnetic Cataclysmic Variables, ed. S. Vrielmann, & M. Cropper, ASP Conf. Ser., 315, IAU Colloq., 190, 187
Beuermann, K., & Burwitz, V. 1995, in Magnetic Cataclysmic Variables, ed. D. A. H. Buckley, & B. Warner, ASP Conf. Ser., 85, 99
Beuermann, K., Baraffe, I., Kolb, U., & Weichhold, M. 1998, A&A, 339, 518
Kirkpatrick, J. D., & McCarthy, Jr., D. W. 1994, AJ, 107, 333
Knigge, C. 2006, MNRAS, 373, 484
Leggett, S. K., Allard, F., Berriman, G., Dahn, C. C., & Hauschildt, P. H. 1996, ApJS, 104, 117
Osborne, J. P., Giommi, P., Angelini, L., Tagliaferri, G., & Stella, L. 1988, ApJ, 328, L45
Pizzolato, N., Maggio, A., Micela, G., Sciortino, S., & Ventura, P. 2003, A&A, 397, 147
Ramsay, G., & Cropper, M. 2007, MNRAS, 379, 1209
Schmidt, G. D., Szkody, P., Vanlandingham, K. M., et al. 2005, ApJ, 630, 1037
Schwope, A., Hasinger, G., Lehmann, I., et al. 2000, Astron. Nachr., 321, 1
Schwope, A. D., Schwarz, R., Sirk, M., & Howell, S. B. 2001, A&A, 375, 419
Schwope, A. D., Brunner, H., Buckley, D., et al. 2002a, A&A, 396, 895
Schwope, A. D., Brunner, H., Hambaryan, V., & Schwarz, R. 2002b, in The Physics of Cataclysmic Variables and Related Objects, ed. B. T. Gänsicke, K. Beuermann, & K. Reinsch, ASP Conf. Ser., 261, 102
Sion, E. M. 1999, PASP, 111, 532
Szkody, P., Henden, A., Mannikko, L., et al. 2007, AJ, 134, 185
Vogel, J., Schwope, A. D., & Gänsicke, B. T. 2007, A&A, 464, 647
Warner, B. 1995, Cataclysmic variable stars, Cambridge Astrophysics Series (Cambridge, New York: Cambridge University Press)
Watson, M. G., King, A. R., & Williams, G. A. 1987, MNRAS, 226, 867
Zombeck, M. V. 1990, Handbook of space astronomy and astrophysics (Cambridge: University Press), 2nd edn.